Industrial Crops & Products 214 (2024) 118475

Contents lists available at ScienceDirect

Industrial Crops & Products

journal homepage: www.elsevier.com/locate/indcrop

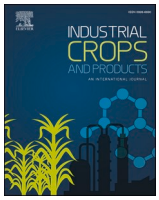

Development of functional graphene oxide-urethane coating systems from *Ricinus communis* seed oil

Samuel Adeboye [a], Oluwafayokunmi Adebamiro [a], Olayemi Arigbede [b], Hesdh Irorevbo [a], Adesola Ajayi [c], Emmanuel Akintayo [d], Kolawole Ajanaku [a], Pratyay Basak [e], Ramanuj Narayan [e], Tolutope Siyanbola [a,e,*]

[a] Department of Chemistry, Covenant University, P.M.B. 1023, Ota, Ogun State, Nigeria
[b] Industrial Chemistry Programme, Bowen University, P.M.B. 284, Iwo, Osun State, Nigeria
[c] Department of Biological Sciences and Biotechnology, Caleb University, Imota, Lagos State, Nigeria
[d] Department of Chemistry, Ekiti State University, P.M.B. 5363, Ado-Ekiti, Ekiti state, Nigeria
[e] Polymers and Functional Materials Division, Indian Institute of Chemical Technology, Hyderabad, Telangana State 500 007, India

ARTICLE INFO

Keywords:
Graphene oxide
Nanoparticles
Antimicrobial
Polyurethane
Ricinus communis
Coating films

ABSTRACT

The surface-modified graphene oxide (GO) nanoparticles and their blending with a fixed percentage of trimethylopropane (TMP) in *Ricinus communis* seed oil were successfully prepared in a one-pot urethane reaction using 4,4′-diisocyanato dicyclohexylmethane (H_{12}MDI) and methyl isobutyl ketone (MIBK) as the reaction solvent. The structural elucidation and surface morphology of pristine and hybrid composites of the polyurethane coating films were investigated with the aid of Fourier transform infrared spectroscopy (FT-IR), Energy-dispersive X-ray spectroscopy (EDX), Proton nuclear magnetic resonance (^{1}H NMR), X-ray diffraction (XRD), and Scanning electron microscope (SEM). The presence of FT-IR absorption peaks at 790 cm^{-1} to 870 cm^{-1}, 990 cm^{-1}, and 1017 cm^{-1} confirms the following functional groups phenyl -CH bend, stretching phenolic -CO, and epoxyl -C-O-C, respectively in modified graphene oxide. An evaluation of the thermal stability of the coating films that were synthesised was carried out with the use of a thermogravimetric analyzer (TGA). It was seen that as the amount of modified graphene oxide in the urethane films increased, so did the water contact angle from 0% to 0.5%. Antimicrobial and anticorrosive properties of the materials were also evaluated.

1. Introduction

The usefulness of polyurethane (PU) in various fields, especially in corrosion prevention, which is a global phenomenon, cannot be overemphasised. However, the synthesis of PU from fossil fuels, which is nonrenewable, has been of great concern to environmentalists. Polyurethanes, a very versatile and extensively utilised industrial material, have been successfully employed in various applications. The utilisation of renewable resources for the synthesis of polyurethane polymeric materials holds substantial economic and ecological importance. Acceptability of these polyurethanes derived from renewable resources is increasing due to the appealing qualities associated with the unique structures of the triglycerides that are found in vegetable oils, along with the environmental and industrial sustainability benefits they offer (Adeboye et al., 2023; Paraskar et al., 2021; Pradhan and Mohanty, 2015). Corrosion is commonly defined as the process by which a material deforms or deteriorates due to its contact with the surrounding environment, such as gas, moisture, and ultraviolet (UV) radiation (Ibrahimi et al., 2021). Mitigation or prevention of corrosion has been a multimillion-dollar global industry (Chauhan et al., 2020). Corrosion is a prominent factor contributing to the failure of process equipment. This can lead to an untimely deterioration of metallic elements, which can cause adverse financial consequences, environmental pollution, and potential harm or fatality (Fu et al., 2020; Ibrahimi et al., 2021). The corrosion phenomenon has also been responsible for a significant loss of human life within the engineering community, leading to substantial financial burdens of billions of dollars (Sunday and Abimbola, 2019). There are many types of corrosion that stakeholders combat daily (Chauhan et al., 2020). Thus, developing durable, affordable, and eco-friendly corrosion inhibition technologies to safeguard infrastructure is an urgent and strategic priority for global economies (Ibrahimi et al., 2021; Kawsihan et al., 2023; Sunday and Abimbola, 2019). Among

* Corresponding author at: Department of Chemistry, Covenant University, P.M.B. 1023, Ota, Ogun State, Nigeria.
E-mail address: tolu.siyanbola@covenantuniversity.edu.ng (T. Siyanbola).

https://doi.org/10.1016/j.indcrop.2024.118475
Received 20 February 2024; Received in revised form 18 March 2024; Accepted 26 March 2024
Available online 9 April 2024
0926-6690/© 2024 Elsevier B.V. All rights reserved.

Table 1
Physicochemical properties of castor oil.

Properties	CSO	TPSO	JCO (Jamiu et al., 2015)
Acid value (mg KOH/g)	3.8831	2.3341	12.50
Iodine value (gI_2/100 g)	82.1281	74.9	102.93
Free Acid Value	1.9415	1.1670	ND
Refractive index (40 ℃)	1.4765	1.4652	1.465
Specific gravity	0.9583	0.9179	0.907
Saponification Value (mg KOH/g)	188.3	194.3	164.79
Moisture content (%)	5.2	2.4	0.091

Table 2
CSO solubility test.

Solvent	Solubility
Chloroform	Soluble
Acetone	Soluble
Xylene	Soluble
Dimethyl sulfoxide (DMSO)	Soluble
4-methyl pentan-2-one, also known as methyl isobutyl ketone (MIBK)	Soluble
Diethyl ether	Soluble
Toluene	Soluble
Methanol	Soluble
Ethanol	Sparingly soluble
Water	Not soluble
1,4-Dioxane	Soluble

the most prevalent approaches employed for corrosion prevention are anti-corrosion coatings and corrosion inhibitors. Corrosion inhibitors (CI) are widely employed in mitigating general and pitting corrosion (Chauhan et al., 2020). Hydrophobic coatings are a surface treatment that repels water extraordinarily, thus inhibiting corrosion (Ahmad et al., 2018). These coatings are designed to create a highly water-repellent surface by reducing the contact area between water droplets and the coated surface, resulting in the droplets rolling off or bouncing off the surface (Bai et al., 2021). There are numerous natural superhydrophobic surfaces, including plant and insect surfaces., like the lotus plant and the chitinous cuticle of crustaceans. Paint is inherently hydrophilic and susceptible to contamination by waterborne pollutants, and due to this hydrophilic nature, paint attracts water and dirt. Consequently, the paint's visible appearance deteriorates, giving it an aged and dirty look (Ahmad et al., 2018). However, applying polyurethane coatings in virtually every industry has generated research interest in introducing nanoparticles (especially their modified forms) into polymeric matrices, thereby improving the hydrophobicity of the composites (Das and Mahanwar, 2020). Modified nanoparticles that have shown such hydrophobic properties in urethane systems are graphene oxide (GO), Zinc oxide (ZnO) (Siyanbola et al., 2013), Titanium (iv) oxide (TiO_2) (Siyanbola et al., 2021), etc. Graphene is a flat, single-layer arrangement of carbon atoms connected by covalent bonds in an SP^2 hybridization pattern. These carbon atoms are arranged in a hexagonal lattice, forming a honeycomb-like network (Sun, 2019; Yu et al., 2020). As a monolayer allotrope of carbon, graphene functions as the fundamental building block for several other carbon-based allotropes (Adetayo and Runsewe, 2019); thus, graphite flake, which is an intrinsic mineral that occurs naturally, undergoes a purification process for the removal of heteroatomic impurities. Graphite is an inorganic element commonly regarded as a mineral that can be used to synthesise graphene oxide through the oxidation process. This method facilitates the addition of functional groups that contain oxygen, which has the beneficial characteristic of being easily dispersed in water (Han et al., 2020). These functional groups boost the hydrophilicity of GO and facilitate its dispersion in solvents, hence facilitating its integration into composite materials (Jena and Philip, 2022). In addition, the inherent hydrophilic nature of graphene oxide enables its homogeneous deposition onto many surfaces, forming thin films (Marcano et al., 2010). Graphene oxide has properties that are different from graphene, such as reduced electrical conductivity and increased solubility (Adetayo and Runsewe, 2019). Other distinctive characteristics of GO are good mechanical strength, a high aspect ratio, and a large surface area (Duong et al., 2020). These inherent features of GO render it a promising material for application in coatings to enhance its hydrophobicity (Crawford and Escarsega, 2000).

Furthermore, one crucial consideration is that hydrophobic surfaces must possess a textured structure to maintain their hydrophobic properties for an extended period, enabling them to exhibit longevity and durability over time (Adetayo and Runsewe, 2019). Previous works showed that incorporating modified graphene oxide (GO) into the polyurethane (PU) coating can greatly improve the mechanical properties and the thermal stability of the polyurethane/graphene oxide polymer (Alrashed et al., 2019), but no work has been done with the unique combination of castor seed oil (CSO), trimethylolpropane (TMP) and GO. In this study, the GO is incorporated into functional polymer nanocomposite coatings as a reinforcing nanofiller to enhance mechanical, thermal, barrier, and electrical properties at low dosages of 0.1 wt%, 0.3 wt%, and 0.5 wt%. For the first time, this research details the successful development of a graphene oxide-reinforced polyurethane hybrid coating with TMP and castor seed oil for superior anticorrosive performance combined with enhanced mechanical durability and thermal stability. The synergistic integration of the passive barrier protection afforded by the graphene oxide nanoplatelets, along with the hard segments and crosslinked network structure of the polyurethane polymer matrix, resulted in a structurally robust yet flexible surface treatment.

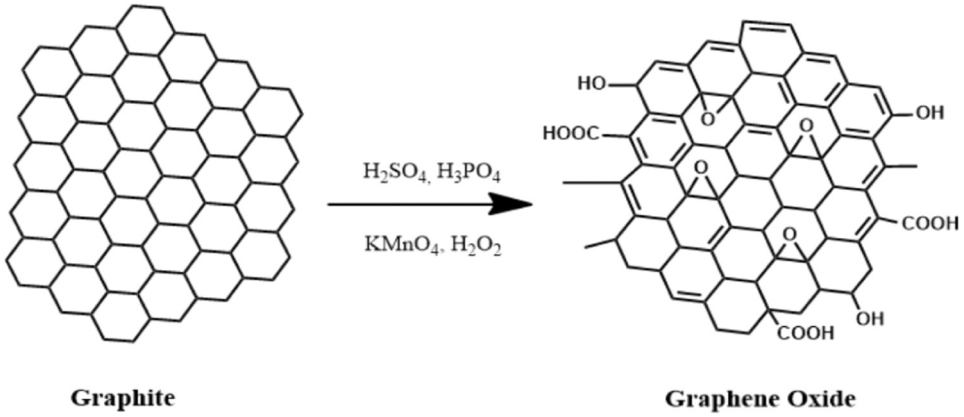

Fig. 1. Synthesis of graphene oxide.

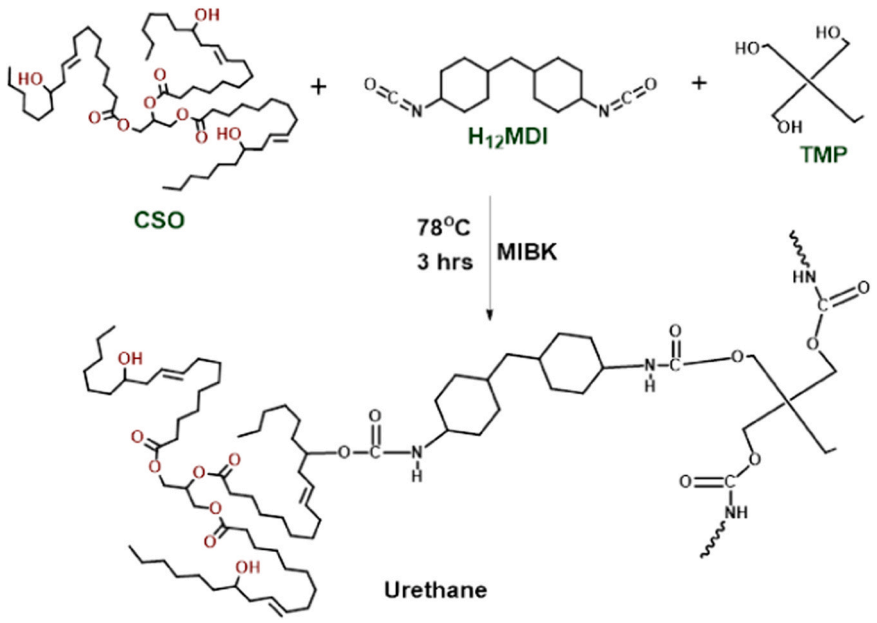

Fig. 2. Synthesis of CSO-TMP Polyurethane.

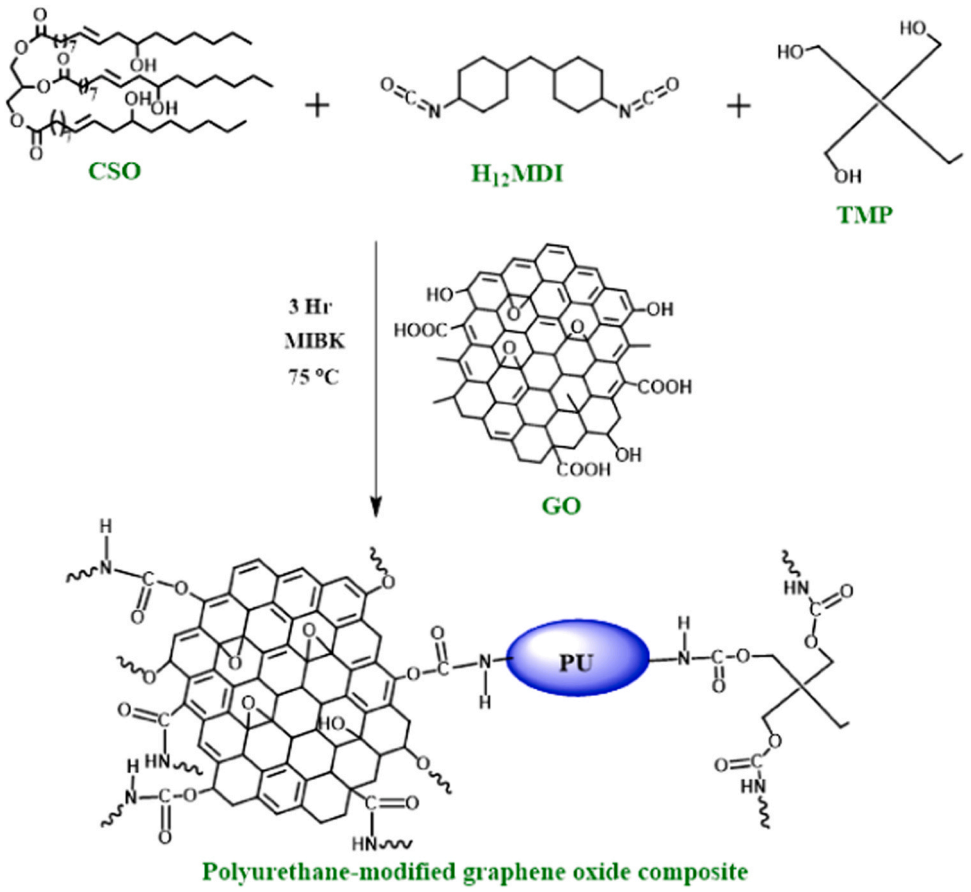

Fig. 3. One-pot synthesis of hybrid PU-GO composite coating.

2. Experimental

2.1. Material and methods

Castor seed oil (CSO) obtained from Ado-Ekiti, Southwestern Nigeria, was extracted as previously reported (Siyanbola et al., 2023). 4, 4′-Diisocyanato dicyclohexylmethane (H_{12}MDI) was obtained from Sigma-Aldrich, USA. Trimethylolpropane (TMP), sulphuric acid (H_2SO_4), and phosphoric acid (H_3PO_4) were also products of Sigma-Aldrich, USA. Graphite powder was acquired from Swift Services,

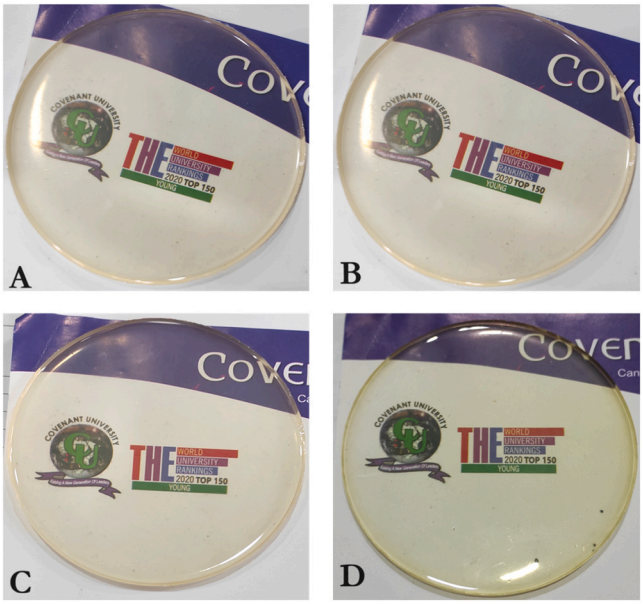

Fig. 4. Photographic showing the retention transparency test of coatings, A= PU, B= 0.1% PU-GO, C= 0.3% PU-GO, D= 0.5% PU-GO.

India. Potassium permanganate ($KMnO_4$), hydrogen peroxide (H_2O_2), and 4-methyl pentan-2-one (MIBK) were purchased from Merck Chemicals, Germany.

2.2. Preparation of castor seed oil

Castor *(Ricinus communis)* seed oil was extracted from the castor seed beans by the solvent extraction method using n-hexane with the aid of a Soxhlet extractor. Heat was applied to bring the solvent to boiling at about 67–68 ℃, while refluxing with water for four hours. The solvent was recovered using a rotary evaporator (Siyanbola et al., 2023). The vegetable oil was appropriately labelled and stored at room temperature.

2.3. Synthesis of graphene

Graphene oxide was synthesised using a modified hummers approach, as documented in the previous studies (Alam et al., 2017; Zaaba et al., 2017). A mixture of H_2SO_4 (27 ml) and H_3PO_4 (3 ml) was prepared in a ratio of 9:1. The resulting mixture was agitated under a fume cupboard. A quantity of graphite powder weighing 0.225 g was introduced into the mixture while constantly stirring. $KMnO_4$ (1.32 g) was then progressively added to the solution. The blend was continuously agitated for 6 hours till the emergence of an olive-green colouration was observed. A solution of hydrogen peroxide (0.675 ml) was added drop wisely to remove excess potassium permanganate ($KMnO_4$). The mixture was subjected to additional agitation for 10 minutes. The reaction setup was allowed to undergo a cooling process because the ongoing reaction exhibited exothermic characteristics. 10 ml of hydrochloric acid and 30 ml of deionized water were introduced. The resultant mixture was centrifuged for 7 minutes.at a rotational speed of 5000 revolutions per minute. The supernatant was decanted, and the remaining residue was rinsed three times with hydrochloric acid and deionized water. The resultant black graphene oxide was dried at 90 ℃. in a hot air oven for 24 hours.

2.4. Synthesis of castor seed oil polyurethane and hybrids

CSO (5 g), trimethylolpropane (TMP) (10% wt.), and the calculated amount of GO nanoparticles in varying percentages were measured and

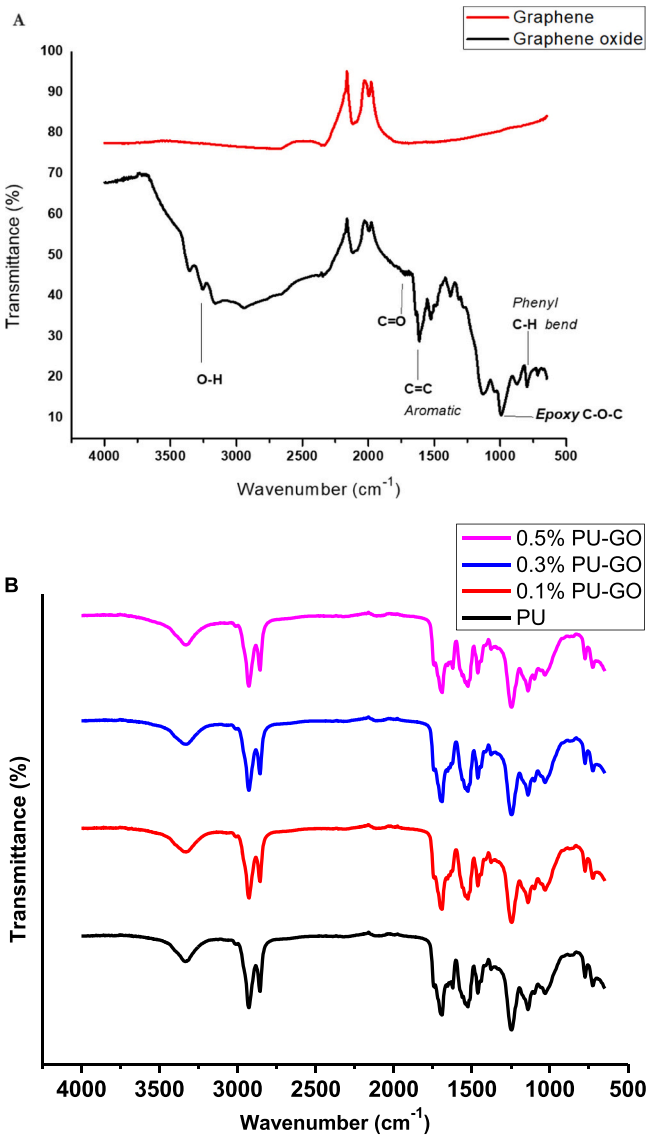

Fig. 5. FTIR spectra: (a) Overlay of graphene and its modified oxide (b) Spectra of PU and its hybrid films.

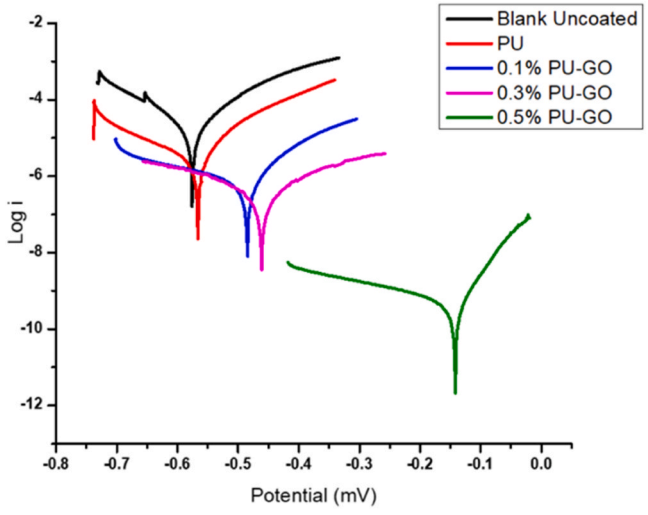

Fig. 6. Tafel plot.

Table 3
Electrochemical parameters.

Samples	Corrosion rate (mm/year) R_{corr}	Polarization Resistance R_p ($K\Omega cm^{-2}$)	E_{corr}, (mV)	I_{corr} (A/cm^2)
Blank (Uncoated)	0.12362	1.40×10^{3}	-0.57659	1.06×10^{-5}
PU	0.029142	8.21×10^{3}	-0.56716	2.51×10^{-6}
0.1% PU-GO	0.0051022	4.38×10^{4}	-0.48564	4.39×10^{-7}
0.3% PU-GO	0.0028171	1.13×10^{5}	-0.46187	2.42×10^{-7}
0.5% PU-GO	3.13×10^{-6}	5.08×10^{7}	-0.14219	2.69×10^{-10}

Fig. 7. Water contact angle of A= PU, B= 0.1% PU-GO, C= 0.3% PU-GO, D= 0.5% PU-GO.

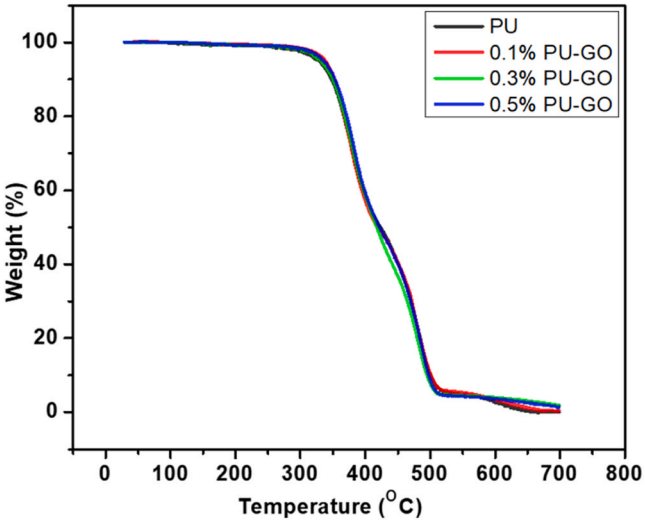

Fig. 8. Combined TGA of the PU samples.

Table 4
Dissociation Temperatures.

Sample	Urethane Dissociation Temperature	Ester Dissociation Temperature
0.0% PU-GO	232.425–383.077	488.768 – 531.589
0.1% PU-GO	253.835–384.440	489.157 – 533.730
0.3% PU-GO	263.373–386.775	493.050 – 535.092
0.5% PU-GO	364.151–389.306	494.023 – 544.824

poured into approximately 10 ml of 4-methyl pentane-2-one. The solution was subsequently subjected to sonication treatment at 50 ℃ for one hour. A 250 ml three-neck round bottom flask was fitted with a nitrogen gas inlet, thermometer, and dropping funnel. Dissolved 3 g of 4,4′-diisocyanato dicyclohexylmethane (H_{12}MDI) in 5 ml of 4-methyl pentan-2-one. The resulting solution was introduced into the flask while stirring continuously. After sonication, the mixture was carefully transferred into the three-neck round bottom flask using a dropwise method. This reaction procedure was maintained at 75–78 ℃for 3 hours. The reaction's advancement was assessed throughout this period using thin-layer chromatography (TLC). Upon completion of the reactions, the films were carefully applied and thinly spread onto silicon moulds and subsequently allowed to cure naturally at room temperature. The cured films were carefully removed from the mould by peeling. The films are then labelled as polyurethane (PU), polyurethane-graphene oxide (PU-GO) (0.1 wt./%), PU-GO (0.3 wt./%), and PU-GO (0.5 wt./%).

2.5. Characterization

The methodologies employed for the physicochemical characterisation of the extracted oil were modified from those established by the American Oil Analytical Chemists (AOAC). Structural elucidation was performed with CARY 630 FTIR spectrophotometer by Agilent Technologies USA for FTIR and Nanalysis model X685 by Nanalysis Corporation, Canada, for ^{1}H NMR analyses. Scanning Electron Microscope (SEM) imaging and Energy-dispersive X-ray spectroscopy (EDX) compositional analysis using Hitachi TM 4000PLUS SEM Japan carried out the morphological investigation of the surfaces. A Simultaneous Thermal Analyzer (STA6000) [PerkinElmer Inc. USA] was used to perform both Thermogravimetric analysis (TGA) and DSC analyses simultaneously under an inert argon atmosphere, heating the samples from room temperature to 800 ℃ at a rate of 10 ℃/min and a gas flow rate of 20 cm^3/min. Also, Texas USA Siemens D5000 X-ray diffraction (XRD) was used to measure the X-ray diffraction. The water contact angle test was conducted with a Goniometer (model-IL4201 DSA) from Krüss GmbH, Germany. A salt mist chamber was used to conduct the salt spray testing following ASTM B 177–94 standards. A 3.5 wt% NaCl solution was atomized by compressed air in the specimen chamber. *In vitro* investigation and evaluation of the antimicrobial activities of the synthesized polymers were carried out against *Rhizopus stolonifera*, *Aspergillus niger*, Gram-positive organisms; *Staphylococcus aureus* (MTCC 96), *Bacillus subtilis* (MTCC 441) and Gram-negative organisms; *Escherichia coli* (MTCC443) (Siyanbola et al., 2015). Antimicrobial assessments were conducted by observing the reduction in the growth of microorganisms under and around films presented on substrates consisting of agar medium. Each treatment was replicated three times. The MTCC is a collection of microbiological samples maintained at IMTECH (CSIR LAB) in Chandigarh, India (Siyanbola et al., 2013)

2.6. Electrochemical test (Tafel method)

Corrosion resistance was studied by plotting the Tafel graph on Origin 8.5 software from the data collected from Autolab B.V. Potentiostat/galvanostat PGSTAT302N by Metrohm Netherlands. A conventional three-electrode cell was used for the electrochemical studies, with 3.5% NaCl solution at pH 7.0 as the electrolyte. An electrochemical cell arrangement was utilised, which included a working electrode comprising a mild steel panel (1 cm x 1 cm x 0.2 cm) coated with a polymer film. While the reference is an uncoated mild steel panel of similar dimensions (1 cm x 1 cm x 0.2 cm). The corrosion rate potential (E_{corr}) was set at 200 mV while the current density (I_{corr}) was set at 5 mV/min. The corrosion current densities (I_{corr}) were estimated by identifying the intersection point of a linear segment when a straight line is drawn along the cathodic or anodic curve and extending it to the corrosion potential (E_{corr}). Tafel plots were employed to determine polarisation resistance (Rp). The electrochemical study was performed in a three-electrode electrochemical device to determine the corrosion resistance property of the polymer films using the Tafel extrapolation method (Poursaee, 2010; Raghupathy et al., 2017).

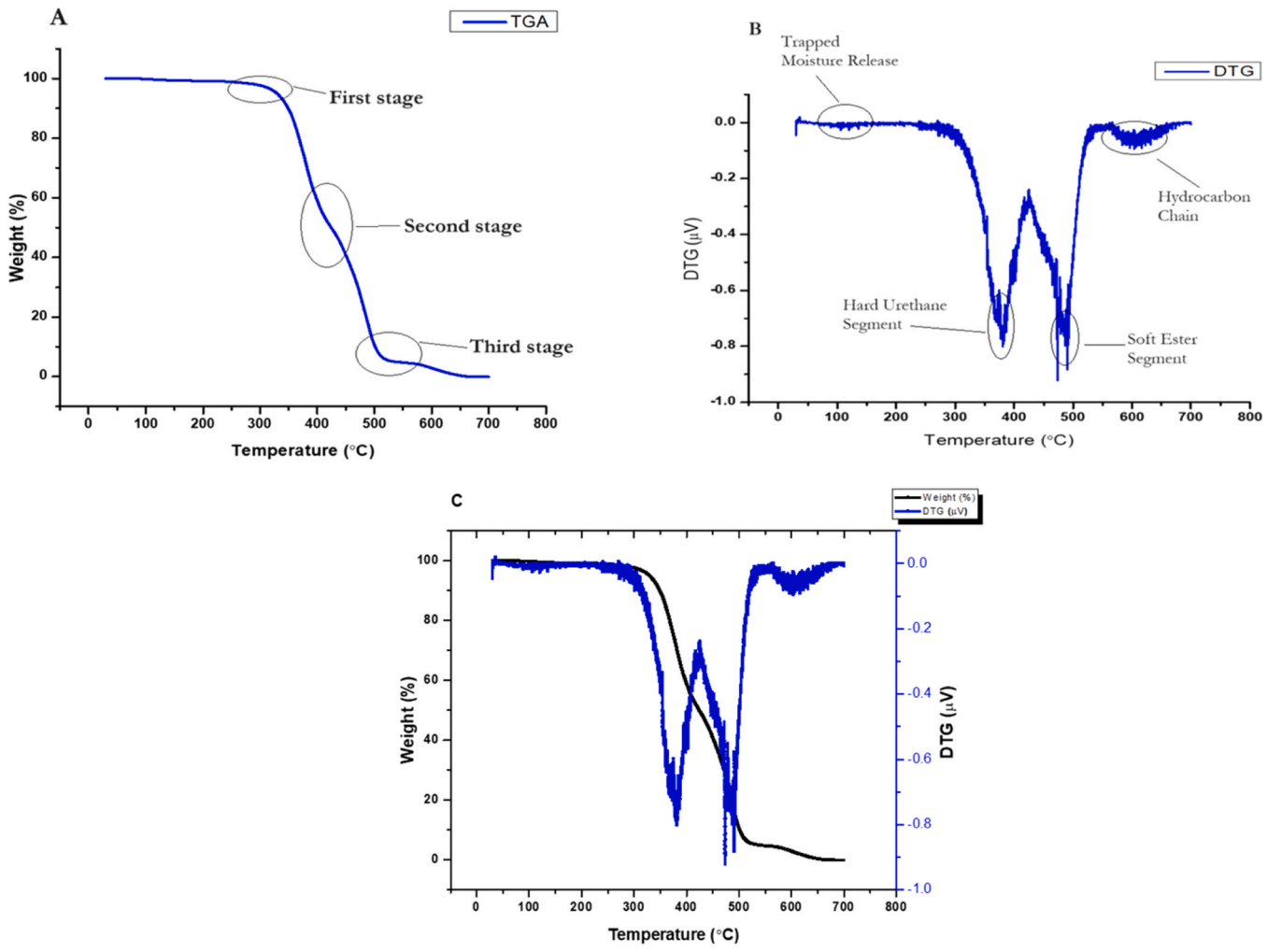

Fig. 9. (A) TGA, (B) Derivative of TG, and (C) Combined plot of TGA and DTG.

3. Results and discussion

3.1. Physico-chemical characteristics

Table 1 shows the comparison of the physicochemical analyses of CSO, *Thevetia peruviana* seed oil (TPSO), and *Jatropha curcas* oil (JCO) [28], CSO and TPSO are both non-drying seed oils (owing to their iodine values less than 115 gI/100 g (Siyanbola et al., 2023), the contrary is that of JCO having the highest of iodine value of the three oils under investigation. However, the lower acid value of CSO (3.8831 mg KOH/g) indicates that the oil is less prone to rancidity when exposed to air, moisture, light, or bacterial action, which could shorten its durability over time (Siyanbola et al., 2023). The CSO saponification value of 188.3 mg KOH/g indicates the oil usage for liquid soap, shaving creams, and shampoos. The 1.4765 refractive value reflects the saturation value of the oil. The solubility profile of CSO is presented in Table 2. The pictorial representation of synthesised films is presented in Fig. 4. The photographic figure shows the vivid clarity and transparency of all the coating films.

3.2. Synthesis of graphene oxide (GO)

According to Fig. 1, GO was successfully synthesised from the graphene nanoparticles as depicted by the presence of Carbonyl (−C═O), hydroxyl (−OH), carboxyl (−COOH), and epoxy (C−O−C) functional groups, which rendered it hydrophilic. This was established by the spectrum of FTIR, as seen in Fig. 5A. The FTIR absorption peaks corresponding to several functional groups are distinctly visible in Fig. 5A. The spectrum of graphene oxide (GO) material shows phenyl C-H bend (790 and 870 cm^{-1}), C-OH (1375 cm^{-1}), phenolic C-O stretch (990 cm^{-1}), epoxy C-O-C (1017 cm^{-1}), C═C stretch of the aromatic ring (1610 cm^{-1}). The peak at 1719 cm^{-1} indicates the stretching vibrations of the C═O bond in carboxylic acid, while that of 2925 cm^{-1} represents the OH bond present in COOH. The broad peaks between the 3150 cm^{-1} and 3700 cm^{-1} regions correspond to phenolic -OH or -OH groups derived from carboxylic groups. All these peaks distinguish the graphene oxide (GO) spectrum from that of graphene.

3.3. Synthesis of polyurethane and hybrid polyurethanes

Fig. 2 shows that the CSO and TMP, which contain hydroxyl (OH) groups, react with H_{12}MDI, which contains two isocyanate (-NCO) groups. The NCO groups of H_{12}MDI react with the OH groups on CSO and TMP, forming urethane links (-NH-CO-O-). TMP serves as an additional multifunctional polyol to crosslink with H_{12}MDI and increase the crosslink density of the resulting polyurethane. The multiple hydroxyl groups on TMP allow more urethane linkages to form during the polymerisation with H_{12}MDI, generating the polyurethane polymer chain with CSO as the backbone that links H_{12}MDI moieties. Fig. 3 shows that graphene oxide nanosheets are incorporated as a reinforcement filler to improve polyurethane's electrical, thermal, and corrosion resistance qualities, as well as its mechanical properties. The synthesis proceeds via

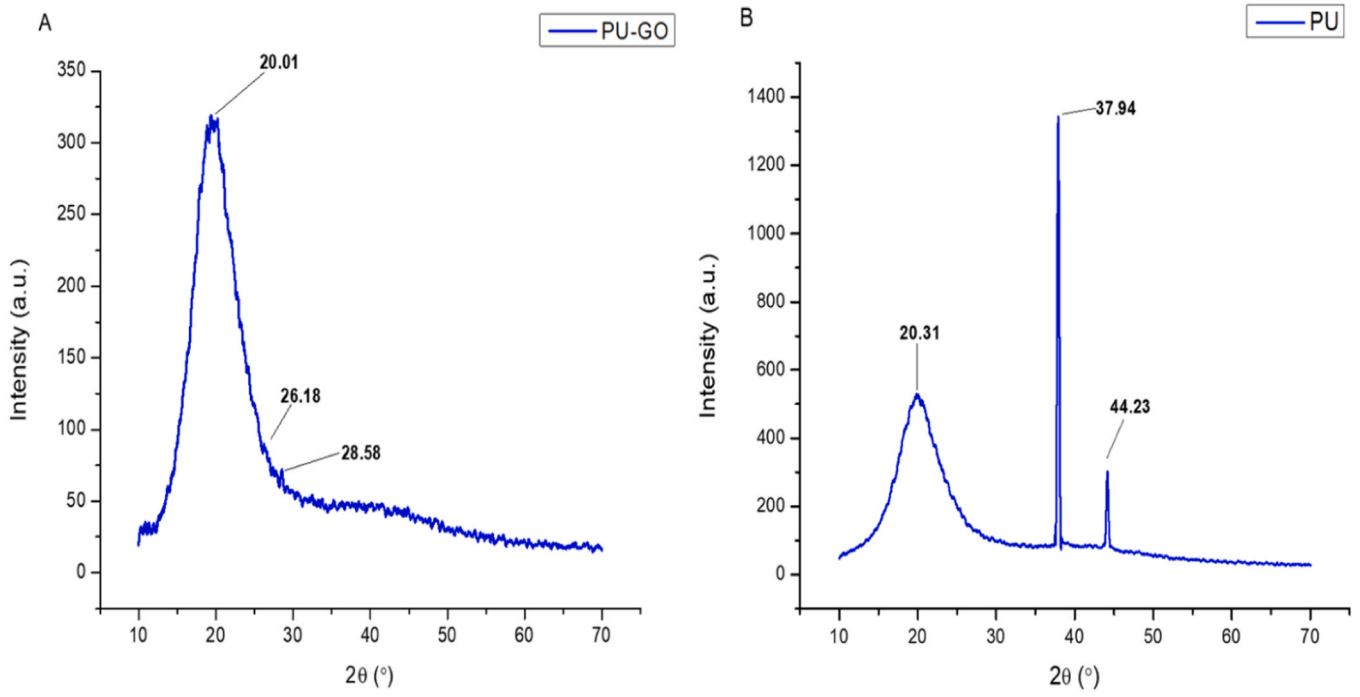

Fig. 10. X-ray diffraction patterns of A = PU-GO and B = PU.

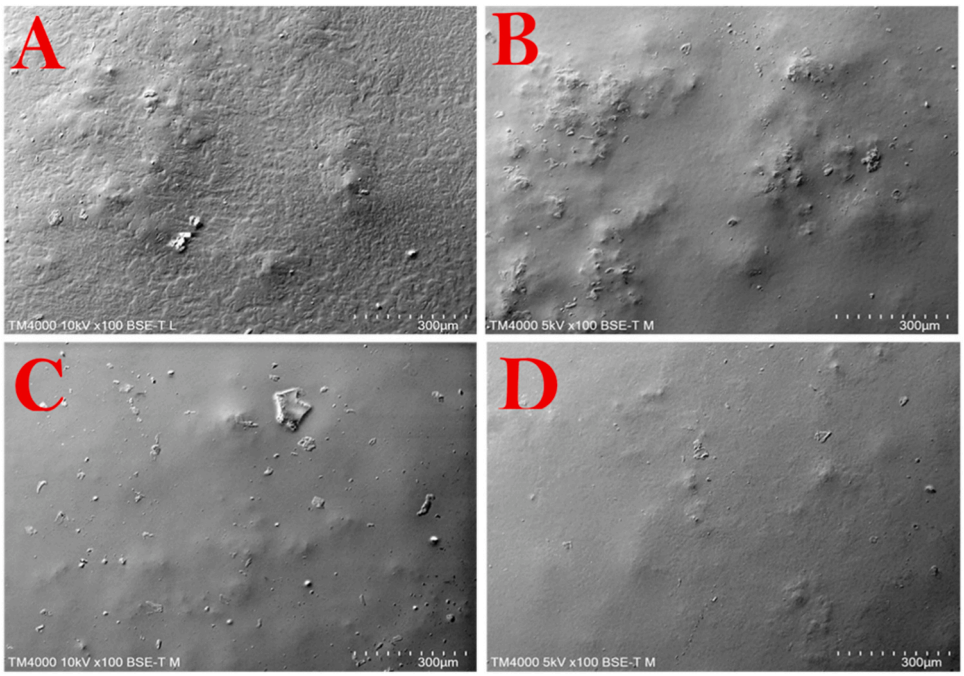

Fig. 11. SEM micrograph of coating films.

step-growth polymerisation as the hydroxyl and isocyanate groups react to form urethane linkages, incorporating castor oil, TMP, and GO into a crosslinked H_{12}MDI-derived polyurethane with enhanced properties from the nanofiller (Fig. 4). The bands that are distinctive of urethane in the PU-GO material are depicted in Fig. 5B. –N–H stretching at 3332 cm^{-1}, the peak at 2855 cm^{-1} is for symmetric -CH_2 while the peak at 2929 cm^{-1} is for asymmetric -CH_2, The C═O of the carbonyl group appeared at 1692 cm^{-1}, also the C-O of urethane is seen at 1244 cm^{-1}. The absence of any peak between 2000 cm^{-1} and 2200 cm^{-1} indicates a complete consumption of the NCO group. No unreacted NCO was left over in the reaction process. The major distinction between the coatings that contain graphene oxide and the ones that do not is that all the samples that have graphene oxide, as found in Fig. 5B, show a =C-H bend at 790–870 cm^{-1}, which is characteristic of the presence of aromatic rings. This peak is absent in the coating that does not have graphene oxide (0% GO). This result suggests that the chemical composition of polyurethane coatings remained materially unaltered within the examined concentration range of GO.

Table 5
Drying time and Chemical resistance of PU and PU-GO composites.

Code	PU	PU-GO 0.1 wt %	PU-GO 0.3 wt %	PU-GO 0.5 wt %
Drying time[a] (day)	5	4	2	2
H_2O (10 days)	A	A	A	A
EtOH (20% 7 days)	A	A	A	A
NaOH (5%, 2 h)	C	C	A	A
HCl (5% 10 days)	B	B	A	A

A = unaffected, B = slightly loss of gloss, C = partial removal of film, a = ambient temperature

3.4. Electrochemical test (Tafel method)

The Tafel plot in Fig. 6 analyzes and evaluates electrochemical properties. The potential is depicted along the X-axis of the graph, while the logarithm of the current density is shown along the Y-axis. Applying graphene oxide and polyurethane (PU-GO) composite coatings on mild steel substrates (1 cm x 1 cm x 0.3 cm) resulted in a discernible movement toward the direction of decreased current densities in both the anodic and cathodic branches. This downward shift in current densities indicates detected corrosion process inhibition.

Critical electrochemical parameters for the coatings that corroborate the Tafel plot are presented in Table 3. Corrosion rate (R_{corr}), Polarization Resistance (R_p), E_{corr}, and I_{corr} values from the table indicate an inverse relationship between the polarization resistance and corrosion rate. There was a correlation between a decrease in the rate of corrosion and an increase in the amount of graphene oxide that was incorporated into the polymer. E_{corr} and I_{corr} are useful tools that enable us to assess and compare corrosion resistance in coated materials. When the E_{corr} value is higher, it implies that the corrosion resistance is higher, however, when the I_{corr} value is lower, it suggests that the corrosion resistance is higher. They both confirmed that the corrosion resistance of graphene oxide grows in proportion to its percentage in the PU-GO composite matrix increases.

3.5. Water contact angle

Further confirmation that the GO has been incorporated into the polymer matrices and its effects on the ability of the coatings to repel water was presented by the water contact angle test (Fig. 7). The angle increases with an increase in the amount of the GO from 70℃ for the pristine to 76.5° for the sample with 0.5% GO. This, as a measure of corrosion resistance, demonstrated that the polymers with GO make better corrosion-resistant coatings.

Table 6
Microbial Activities.

Organisms	PU	0.1% PU-GO	0.3% PU-GO	0.5% PU-GO
Bacillus subtilis	-	-	-	-
Escherichia coli	+	++	++++	++++
Staphylococcus aureus	+	+++	+++	++++
Aspergillus niger	-	-	+	+
Rhizopus stolonifer	+	++	+++	++++

- Inactive, + poorly active, ++ Mildly active, +++ Fairly active, ++++ Moderately active

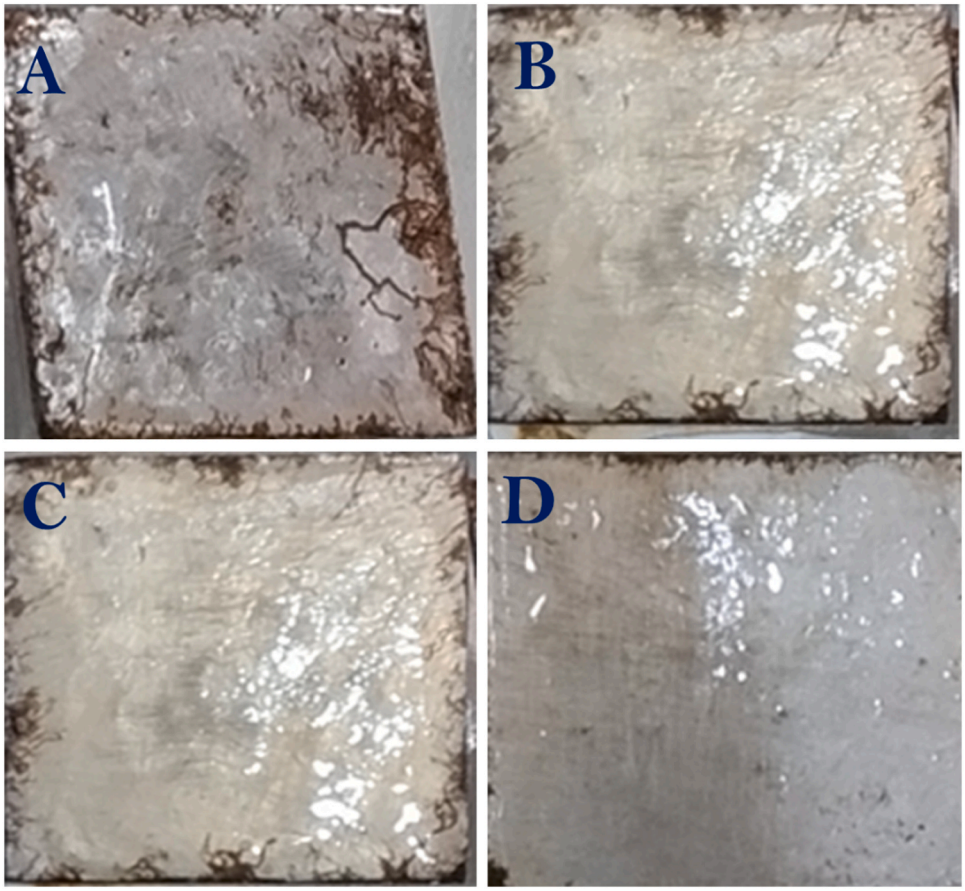

Fig. 12. The 680 hours salt spray results of hybrid coatings in 3.5% NaCl solution.

3.6. Thermogravimetric (TGA) and first derivate of thermogravimetric analyses (DGT)

The specimens were subjected to a controlled heating process in crucibles. The temperature was increased gradually from room temperature to 800 ℃, at the heating rate of 10 ℃/min in an inert argon environment. A gas flow rate of 20 cm^3/min was maintained during the heating process. The TGA and DTG indicated a three-phase degradation of the polymer films, as shown in Fig. 8 and 9. A critical study of the spectra showed that entrapped water molecules and the volatile solvents were released from around 86 ℃ to 124 ℃. while the hydrocarbon residues were released between 570 ℃ and 660 ℃. The initial stage of thermal decomposition, which corresponds to the glass transition stage (T_g), involves the breakdown of urethane bonds. This initial phase of decomposition is likely attributed to the dissociation of isocyanate and alcohol. The dissociation of ester bonds may be responsible for the second degradation step, while the third stage is probably due to the release of the hydrocarbon residues. The downward slope of the DTG thermogram indicates that the degradation stages are endothermic reactions. The finding is in tandem with previously reported three-stage degradation of polymer films (Siyanbola et al., 2015). Table 4 shows that the dissociation temperature increases with the amount of GO embedded in the films.

3.7. X-Ray diffraction

An intense broad peak observed at $2\theta = 20.01^\circ$ in Fig. 10A occurred at $2\theta = 20.31^\circ$ in Fig. 10B, confirming the amorphous nature of the composite polymers. The smaller peak observed at $2\theta = 26.18^\circ$ in Fig. 9A, which signifies the existence of graphene within the PU-GO composite films, is absent in Fig. 10B. Rather, two sharp and intense peaks were seen at $2\theta = 37.94^\circ$ and 44.23°. The spectra confirmed that polymers with consistent microcrystalline structures were formed.

3.8. Morphological analysis with SEM

The SEM micrographs in Fig. 11 showing that A, B, C, and D, represent 0%, 0.1%, 0.3 & 0.5% GO, respectively. The polyurethane films showed that adding graphene oxide resulted in improved homogeneity of dispersion within the polymer matrix. The occurrence of lumps or aggregation was found to be more pronounced in samples A and B, while it significantly diminished in sample D, which contains the highest concentration of graphene oxide. The results obtained from the SEM experiment demonstrated the presence of surface roughness, which appeared to be induced by incorporating graphene oxide (GO) into the polymer matrices.

3.9. Drying behaviour and salt spray evaluation

Table 5 summarizes the time it took for the pristine polyurethane (PU) to dry, its resistance to chemical testing, and the hybrid resin systems (PU-GO) that were coated on glass plates. The doped polymeric composite coatings were seen to dry faster than that of the pristine urethane. This effect improved with a greater percentage composition of graphene oxide.

The rapid drying of the hybrid resin on the activated mild steel substrate is attributable to the network within the polymer matrix, resulting in a denser and more compact system. Glass plates that had been previously coated were placed in 250 ml beakers filled with 200 ml of various chemical media, as shown in Table 5 at 28 ± 5 ℃. Most of the glass plates under investigation showed stable condition (i.e., plates in water and ethanol). However, partial loss of gloss is observed in a medium soaked in 5% NaOH. The existence of an ester group that can be hydrolyzed by alkalis explains this finding. Fig. 12 shows the corrosion investigation of the coated mild steel panels in the salt spray chamber. After 680 hours of salt fog spray in a 3.5% NaCl solution, the PU, PU-GO 0.1 wt%, and PU-GO 0.3 wt% coated panels showed edge and surface corrosion, with the pristine panel showing the most effect. However, the PU-GO 0.5 wt% coated panel showed the most resistance compared to other panels under investigation. The result indicates that modified graphene (GO), when incorporated in higher percentages in polymer matrix, improves salt resistance on coated panels

3.10. Antimicrobial test

The pristine film (PU) and its hybrid urethane composites (0.1% PU-GO, 0.3% PU-GO, and 0.5% PU-GO) produced the antimicrobial results presented in Table 6. These were carried out on *Bacillus subtilis*, *Escherichia coli*, *Staphylococcus aureus*, *Aspergillus niger*, and *Rhizopus stolonifera* test organisms. The film with the highest modified material (i.e., 0.5% PU-GO) showed the best activity against test organisms, while the pristine urethane had the least activity. *Bacillus subtilis* grew overall in test samples, but poor activity was also observed with 0.3% PU-GO and 0.5% PU-GO.

4. Conclusion

The inorganic primary status of graphene was successfully modified into graphene oxide (hybrid) with carboxylic groups at the surface of the material, which was conveniently incorporated into the polymer matrix of the prepared composites. The drying time, chemical resistance, thermal stability, water contact angle, XRD, corrosion studies, and antimicrobial evaluations of synthesised composites were evaluated. It is important to note that the hybrid nanoparticles (GO) enhanced the coating properties of the films. The photographic view of all films examined showed vivid clarity, which did not diminish despite the percentage increase of GO from 0.1 wt% to 0.5 wt%. The antimicrobial activity was zero for *Bacillus subtilis,* and moderate activity was observed with films 0.5 wt% of GO.

CRediT authorship contribution statement

Adesola Ajayi: Writing – review & editing, Resources, Project administration, Methodology, Investigation, Formal analysis. **Hesdh Irorevbo:** Resources, Methodology, Formal analysis. **Olayemi Arigbede:** Resources, Methodology, Data curation. **Oluwafayokunmi Adebamiro:** Methodology, Investigation, Data curation. **Samuel Adeboye:** Writing – original draft, Resources, Methodology, Investigation, Formal analysis, Data curation. **Tolutope Siyanbola:** Writing – review & editing, Writing – original draft, Visualization, Validation, Supervision, Software, Project administration, Methodology, Investigation, Data curation, Conceptualization. **Ramanuj Narayan:** Writing – review & editing, Validation, Supervision, Resources, Project administration, Methodology, Investigation, Formal analysis. **Pratyay Basak:** Writing – review & editing, Visualization, Validation, Supervision, Resources, Project administration, Investigation, Formal analysis, Conceptualization. **Kolawole Ajanaku:** Writing – review & editing, Validation, Supervision, Project administration. **Emmanuel Akintayo:** Writing – review & editing, Visualization, Validation, Supervision, Project administration, Conceptualization.

Declaration of Competing Interest

The authors declare that they have no known competing financial interests or personal relationships that could have appeared to influence the work reported in this paper.

Data availability

No data was used for the research described in the article.

Acknowledgement

Appreciation goes to Covenant University, Ota, Ogun State, Nigeria, for creating a workable platform for this research. The corresponding author (Dr Tolutope O. Siyanbola) is thankful to the Indian Institute of Chemical Technology (IICT), Hyderabad, India for their usual assistance in instrumentation analyses.

References

Adeboye, S.A., Adebowale, A.D., Siyanbola, T.O., Ajanaku, K.O., 2023. Coatings and the environment: a review of problems, progress and prospects, In: IOP Conference Series: Earth and Environmental Science. Institute of Physics. https://doi.org/10.1088/1755-1315/1197/1/012012.

Adetayo, A., Runsewe, D., 2019. Synthesis and fabrication of graphene and graphene oxide: a review. Open J. Compos. Mater. 09, 207–229. https://doi.org/10.4236/ojcm.2019.92012.

Ahmad, D., van den Boogaert, I., Miller, J., Presswell, R., Jouhara, H., 2018. Hydrophilic and hydrophobic materials and their applications. Energy Sources, Part A Recovery, Util., Environ. Eff. https://doi.org/10.1080/15567036.2018.1511642.

Alam, S.N., Sharma, N., Kumar, L., 2017. Synthesis of graphene oxide (GO) by modified Hummers method and its thermal reduction to obtain reduced graphene oxide (rGO) *. Graphene 06, 1–18. https://doi.org/10.4236/graphene.2017.61001.

Alrashed, M.M., Soucek, M.D., Jana, S.C., 2019. Role of graphene oxide and functionalized graphene oxide in protective hybrid coatings. Prog. Org. Coat. 134, 197–208. https://doi.org/10.1016/j.porgcoat.2019.04.057.

Bai, Y., Zhang, Haiping, Shao, Y., Zhang, Hui, Zhu, J., 2021. Recent progress of superhydrophobic coatings in different application fields: an overview. Coatings. https://doi.org/10.3390/coatings11020116.

Chauhan, D.S., Quraishi, M.A., Ansari, K.R., Saleh, T.A., 2020. Graphene and graphene oxide as new class of materials for corrosion control and protection: present status and future scenario. Prog. Org. Coat. https://doi.org/10.1016/j.porgcoat.2020.105741.

Crawford, D.M., Escarsega, J.A., 2000. Dynamic mechanical analysis of novel polyurethane coating for military applications. Thermochim. Acta 357, 161–168.

Das, A., Mahanwar, P., 2020. A brief discussion on advances in polyurethane applications. Adv. Ind. Eng. Polym. Res. https://doi.org/10.1016/j.aiepr.2020.07.002.

Duong, N.T., An, T.B., Thao, P.T., Oanh, V.K., Truc, T.A., Vu, P.G., Hang, T.T.X., 2020. Corrosion protection of carbon steel by polyurethane coatings containing graphene oxide. Vietnam J. Chem. 58, 108–112. https://doi.org/10.1002/vjch.2019000150.

Fu, L., Liao, K., Tang, B., Jiang, L., Huang, W., 2020. Applications of graphene and its derivatives in the upstream oil and gas industry: a systematic review. Nanomaterials. https://doi.org/10.3390/nano10061013.

Han, X., Gao, J., Chen, Z., Tang, X., Zhao, Y., Chen, T., 2020. Correlation between microstructure and properties of graphene oxide/waterborne polyurethane composites investigated by positron annihilation spectroscopy. RSC Adv. 10, 32436–32442. https://doi.org/10.1039/d0ra05872f.

Ibrahimi, B.El, Nardeli, J.V., Guo, L., 2021. An overview of corrosion, In: ACS Symposium Series. American Chemical Society, pp. 1–19. https://doi.org/10.1021/bk-2021-1403.ch001.

Jamiu, J.M., Labunmi, L., Abayomi, A.O., Bodunde, O.J., Ignatius, O.A., 2015. Chemical modification of Jatropha curcas and *Thevetia peruviana* oil as starting materials for chemical industry. Am. J. Sci. Ind. Res. 6, 123–130. https://doi.org/10.5251/ajsir.2015.6.6.123.130.

Jena, G., Philip, J., 2022. A review on recent advances in graphene oxide-based composite coatings for anticorrosion applications. Prog. Org. Coat. https://doi.org/10.1016/j.porgcoat.2022.107208.

Kawsihan, A., Dissanayake, D.M.S.N., Rathuwadu, N.P.W., Perera, H.C.S., Dayananda, K. E.D.Y.T., Koswattage, K.R., Mahadeva, R., Ganguly, A., Das, G., Mantilaka, M.M.M. G.P.G., 2023. Synthesis of an eco-inspired anticorrosive composite for mild steel applications. RSC Adv. 13, 28852–28860. https://doi.org/10.1039/d3ra02857g.

Marcano, D.C., Kosynkin, D.V., Berlin, J.M., Sinitskii, A., Sun, Z., Slesarev, A., Alemany, L.B., Lu, W., Tour, J.M., 2010. Improved synthesis of graphene oxide. ACS Nano 4, 4806–4814. https://doi.org/10.1021/nn1006368.

Paraskar, P.M., Prabhudesai, M.S., Hatkar, V.M., Kulkarni, R.D., 2021. Vegetable oil based polyurethane coatings – a sustainable approach: a review. Prog. Org. Coat. https://doi.org/10.1016/j.porgcoat.2021.106267.

Poursaee, A., 2010. Potentiostatic transient technique, a simple approach to estimate the corrosion current density and Stern-Geary constant of reinforcing steel in concrete. Cem. Concr. Res 40, 1451–1458. https://doi.org/10.1016/j.cemconres.2010.04.006.

Pradhan, S., Mohanty, S., 2015. Synthesis and characterization of renewable resource-based green epoxy coating. Int. J. Chem. Mol. Eng. 9 https://doi.org/10.1999/1307-6892/22086.

Raghupathy, Y., Kamboj, A., Rekha, M.Y., Narasimha Rao, N.P., Srivastava, C., 2017. Copper-graphene oxide composite coatings for corrosion protection of mild steel in 3.5% NaCl. Thin Solid Films 636, 107–115. https://doi.org/10.1016/j.tsf.2017.05.042.

Siyanbola, T.O., Sasidhar, K., Anjaneyulu, B., Kumar, K.P., Rao, B.V.S.K., Narayan, R., Olaofe, O., Akintayo, E.T., Raju, K.V.S.N., 2013. Anti-microbial and anti-corrosive poly (ester amide urethane) siloxane-modified ZnO hybrid coatings from *Thevetia peruviana* seed oil. J. Mater. Sci. 48, 8215–8227. https://doi.org/10.1007/s10853-013-7633-x.

Siyanbola, T.O., Sasidhar, K., Rao, B.V.S.K., Narayan, R., Olaofe, O., Akintayo, E.T., Raju, K.V.S.N., 2015. Development of functional polyurethane-ZnO hybrid nanocomposite coatings from *Thevetia peruviana* seed oil. JAOCS. J. Am. Oil Chem. ' Soc. 92, 267–275. https://doi.org/10.1007/s11746-014-2587-y.

Siyanbola, T.O., Ajayi, A.A., Vinukonda, S., Jena, K.K., Alhassan, S.M., Basak, P., Akintayo, E.T., Narayan, R., Raju, K.V.S.N., 2021. Surface modification of TiO_2 nanoparticles with 1,1,1-Tris(hydroxymethyl)propane and its coating application effects on castor seed oil-PECH blend-based urethane systems. Prog. Org. Coat. 161 https://doi.org/10.1016/j.porgcoat.2021.106469.

Siyanbola, T.O., Adebowale, A.D., Adeboye, S.A., Rao, S.J.V., Ndukwe, N.A., Sodiya, E. F., Ajayi, A.A., Akintayo, E.T., Basak, P., Narayan, R., 2023. Development of functional polyurethane-cenosphere hybrid composite coatings from *Ricinus communis* seed oil. Sci. Afr. 20 https://doi.org/10.1016/j.sciaf.2023.e01711.

Sun, L., 2019. Structure and synthesis of graphene oxide. Chin. J. Chem. Eng. https://doi.org/10.1016/j.cjche.2019.05.003.

Sunday, I.F.O., Abimbola, P.I.P., 2019. Corrosion propagation challenges of mild steel in industrial operations and response to problem definition, In: Journal of Physics: Conference Series. Institute of Physics Publishing. https://doi.org/10.1088/1742-6596/1378/2/022006.

Yu, W., Sisi, L., Haiyan, Y., Jie, L., 2020. Progress in the functional modification of graphene/graphene oxide: a review. RSC Adv. https://doi.org/10.1039/d0ra01068e.

Zaaba, N.I., Foo, K.L., Hashim, U., Tan, S.J., Liu, W.W., Voon, C.H., 2017. Synthesis of graphene oxide using modified hummers method: solvent influence. Procedia Engineering. Elsevier Ltd, pp. 469–477. https://doi.org/10.1016/j.proeng.2017.04.118.